Thin Solid Films 529 (2013) 205–208

Contents lists available at SciVerse ScienceDirect

Thin Solid Films

journal homepage: www.elsevier.com/locate/tsf

Development of a high performance integrated sensor chip with a multi-walled carbon nanotube assisted sensing array

Pi Kai Chuang [a], Li Chun Wang [b], Cheng Tzu Kuo [a,*]

[a] Dept. of Materials Science and Engineering, National Chiao Tung University, Hsinchu 300, Taiwan
[b] Chemical Systems Research Division, Chung-Shan Institute of Science & Technology, Touyan 325, Taiwan

ARTICLE INFO

Available online 12 October 2012

Keywords:
Multi-walled carbon nanotubes
Gas sensors
Toxic gases

ABSTRACT

For room temperature toxic gas sensing, a system chip with a MWCNT (multi-walled carbon nanotube)-assisted array of 30 sensors (two sensors for each of 15 sensor types) was developed. Gases tested include four simulants of chemical warfare agents: dichloromethane, acetonitrile, 2-chloroethyl ethyl sulfide, and dimethyl-methyl phosphonate (DMMP). By selecting 15 different functional polymer materials, each composite sensor composed of 15 sensing stacks (polymer/MWCNTs/Si(001), wafer) was fabricated by a solution droplet casting method to simplify the process. The principle of gas sensing is basically to measure the resistivity change of the composite sensor device upon contact with a target gas. One of the advantages of the sensing stack having a polymer overlayer above the MWCNT layer is being able to protect the MWCNT from direct interaction with the gas to improve sensor life and sensitivity. The results indicate that a fingerprint pattern of the sensor radar plot can be determined for each testing run, and that specificity can be achieved through a 3-D principal component analysis of the radar plots. The results also show that a linear relationship between the resistance response and concentration is clearly evident for these four toxic gases. By extrapolation and careful process monitoring, a sensitivity much lower than 43 ppm for DMMP vapor is likely. The gas sensing mechanisms are discussed in the text.

1. Introduction

Carbon nanotubes (CNTs) are well known as nano-scale quantum object which can exhibit many unique properties for potential nano-device applications [1]. For gas sensing applications, CNT-derived high-sensitivity gas sensors for various gases and nerve agents, such as ammonia, ethanol vapor, NO_2, CO, CH_4, and dimethyl methylphosphonate (DMMP) have been reported [2–4]. In particular, two major types of CNT-assisted chemiresistor sensors have attracted attention in recent years. They are based on inorganic semiconductors [5,6] and organic polymers [7–9]. The sensing mechanism is based on a marked change in dielectric constant or resistivity of the device upon adsorption of the target vapor. Among these gas sensor types, the CNT/functional polymer composite gas sensors appear to provide the following advantages: high gas differentiation at room temperature, high recovery (i.e., analyte desorption) rate, and the ability to be integrated into microstructured sensor designs. [10–16] In this study, a simple gas sensing electrical system chip composed of a 30-sensor array was developed for room temperature sensing. The array includes 15 different composite sensor types, i.e., sensing stacks consisting of multi-walled carbon nanotubes (MWCNTs) and one of the 15 different conductive polymers.

2. Experimental details

2.1. Gas sensing system chip and gas sensor preparation

Fig. 1 shows a stainless steel testing stand with a Si (001) chip consisting of 30 gas sensors and the corresponding 30 independent sensing electrical leads in a 2×15 arrangement to facilitate measurement of the resistance response of each sensor. The chip is 34 mm × 20 mm in size. Each circular membrane sensor is about 2 mm in diameter.

The gas sensors are composed of layer stacks consisting of polymer/MWCNT/Si wafer. Metallic MWCNTs were purchased from XinNano Materials, Inc. and has the following specifications: ~8 nm in diameter, 13 μm in length, and purity > 90%. The polymer materials for this study were selected by considering sensor–analyte interactions with linear solvation energy relationships to insure gas detection specificity [17,18], and with favorable physical adsorption/desorption properties to improve sensor robustness and repeatability. The 15 selected polymer materials are listed in Table 1.

To place each sensor at the desired spot on the chip, a two-step solution droplet method was used, as shown in Fig. 2. First, the electrode layer was prepared by drop-casting a methyl ethyl ketone (MEK) solution (1 wt.% MWCNTs) on the surface of an interdigitized microelectrode (IME) device on the Si wafer, followed by evaporation of the solvent in air at room temperature. The dry MWCNT electrode layer was then cast from an MEK solution containing 1 wt.% polymer which

* Corresponding author. Tel.: +886 937808220.
E-mail address: ctkuo@mail.nctu.edu.tw (C.T. Kuo).

0040-6090/$ – see front matter © 2012 Elsevier B.V. All rights reserved.
http://dx.doi.org/10.1016/j.tsf.2012.09.024

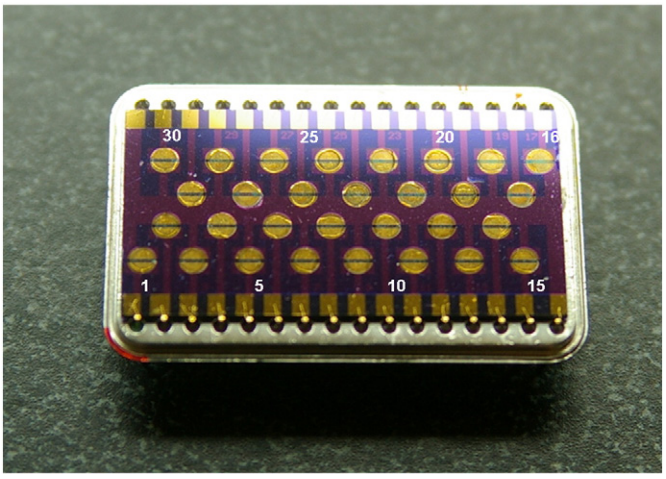

Fig. 1. A stainless steel testing stand installed with electrical leads and an array of 30 gas sensors on an IME device on a Si(001) wafer.

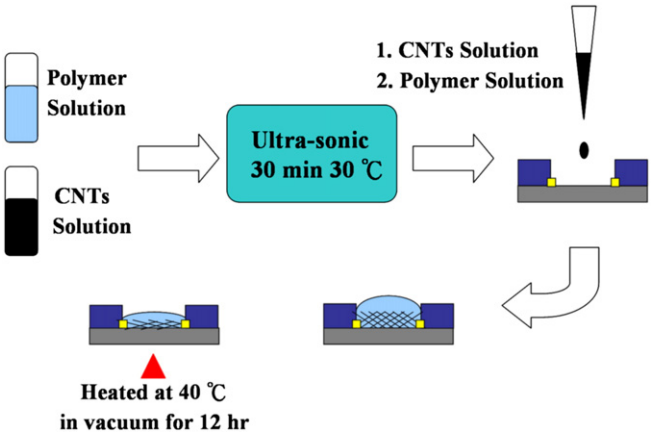

Fig. 2. Schematic diagram showing process steps to prepare the gas sensors on a Si wafer.

was subsequently heated to 40 °C in vacuum for 12 h to form a double layer film, as described elsewhere [19].

2.2. Gas sensing experiments

The tested gases (analytes) include four different chemical warfare agent simulants: dichloromethane (DCM), acetonitrile (ACN), 2-chloroethyl ethyl sulfide (2-CEES), and dimethyl-methyl phosphonate (DMMP). To conduct the gas sensing experiments, the testing stand with sensor array chip was placed in a glass vessel. Analytes with known concentrations were generated by a Standard Gas Generator (made by KIN-TEK Laboratories, Inc.), where the gas concentration was calibrated by measuring the weight loss from the organic solvent solution. The gas flow rate was controlled by a calibrated mass-flow controller (made by Aalborg, Inc.) with air as the carrier gas. For each test, the system stabilized after about 300 s. Analyte at a flow rate of 100 mL/min was then infused into the chamber for 300 s (adsorption), followed by infusing dry air for another 300 s (desorption). After each testing run, the chamber was purged with dry air. Electrical resistance outputs (△R/R %) from each sensor element were measured using a digital multimeter with signals addressed using a multiplexer switch unit. Typical response curves are shown in Fig. 3. "Radar plots" illustrating the sensor response (△R/R %) from 30 sensors (two sensors for each of 15 different sensor types) were obtained, from which the finger print pattern of resistance response (△R/R %) from 30 sensors of 15 sensor types can be determined. Responses of the thirty polymer/MWCNT composite sensors were normalized by the sum of all the sensor response values for the given analytes. This normalization process reduces the dependence of the array response on the vapor concentration and also slightly reduces the effects of sensor drift. By adopting the method of principle component analysis (PCA) of the radar plots, the gas specificity can be enhanced.

3. Results and discussions

3.1. Room temperature sensor response curves

Typical room temperature sensor response (△R/R %) as a function of testing time for determining DMMP gas with concentrations ranging from 43 ppm to 356 ppm by sensor S28 on the chip is shown in Fig. 3. The inset in Fig. 3 is the corresponding sensor peak response as a function of gas concentration. A resistance variation of about 1.6% can be achieved at a concentration of 43 ppm. The inset demonstrates sensor linearity between the measured resistance and the gas concentration, which also was seen for the other 29 composite sensors and the three different volatile organic compound analytes. By monitoring the signal-to-noise(S/N)

Table 1
Polymer materials used in the composite sensor array.

Sensor number[a]	Polymer
S1, S2	Styrene allyl alcohol copolymer
S3, S4	Poly(vinylidene chloride-co-acrylonitrile)
S5, S6	Polyvinylpyrrolidone
S7, S8	Poly(methyl vinyl ether-alt-maleic acid)
S9, S10	Poly(alpha-methylstyrene)
S11, S12	Poly(ethylene adipate)
S13, S14	Poly(vinyl benzyl chloride)
S15, S16	No polymer
S17, S18	Poly(4-vinylphenol-co-methyl methacrylate)
S19, S20	Poly(epichlorohydrine)
S21, S22	Polystyrene
S23, S24	Polycarbonate
S25, S26	Polyethlene glycol
S27, S28	Polyethylene oxide
S29, S30	Ethyl cellulose

[a] Sensor numbers of S1, S2 … correspond to the sensor position numbers of 1, 2 … in Fig. 1, respectively.

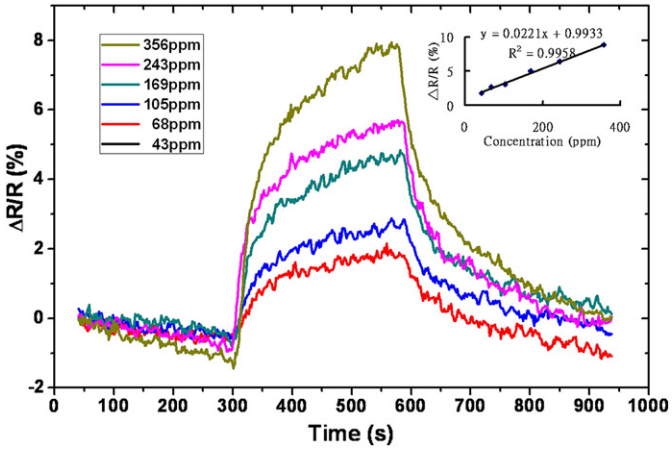

Fig. 3. Room temperature sensor response (△R/R %) versus sensing time curves for DMMP gas at concentrations ranging from 43 ppm to 356 ppm for sensor S28 on the chip. The inset shows the corresponding sensor peak response as a function of gas concentration.

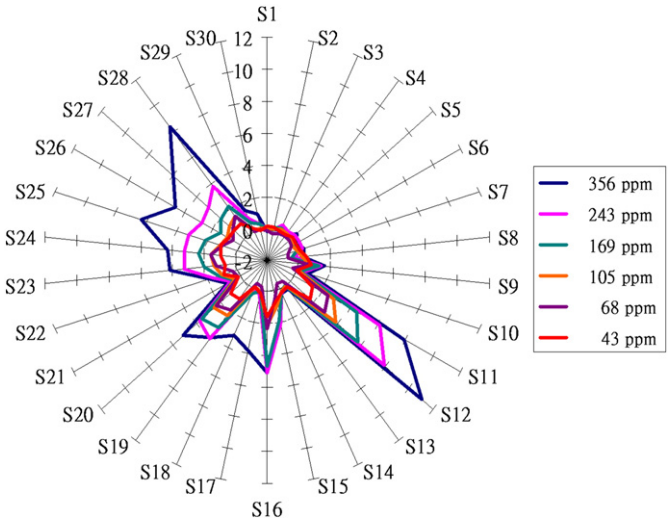

Fig. 4. Radar plots of the room temperature resistance response (△R/R %) of a 30-sensor array exposed to DMMP gas at six different gas concentrations in air.

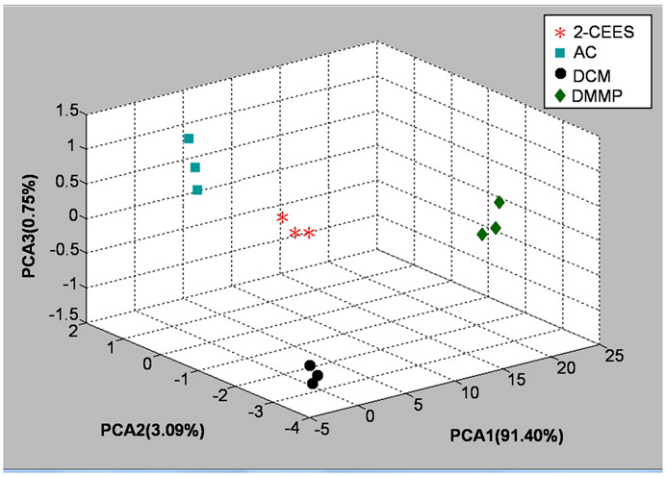

Fig. 6. The 3-D principle component analysis (PCA) plots showing the sensing reproducibility and gas differentiation for four different gases.

ratio of the resistance response and carefully controlling the process and environment, a detection limit much lower than 43 ppm DMMP gas at room temperature can be achieved.

3.2. Effect of gas concentration on sensor response

To construct a library of sensor responses, radar plots for 4 different gases and several concentrations were determined. Typical radar plots

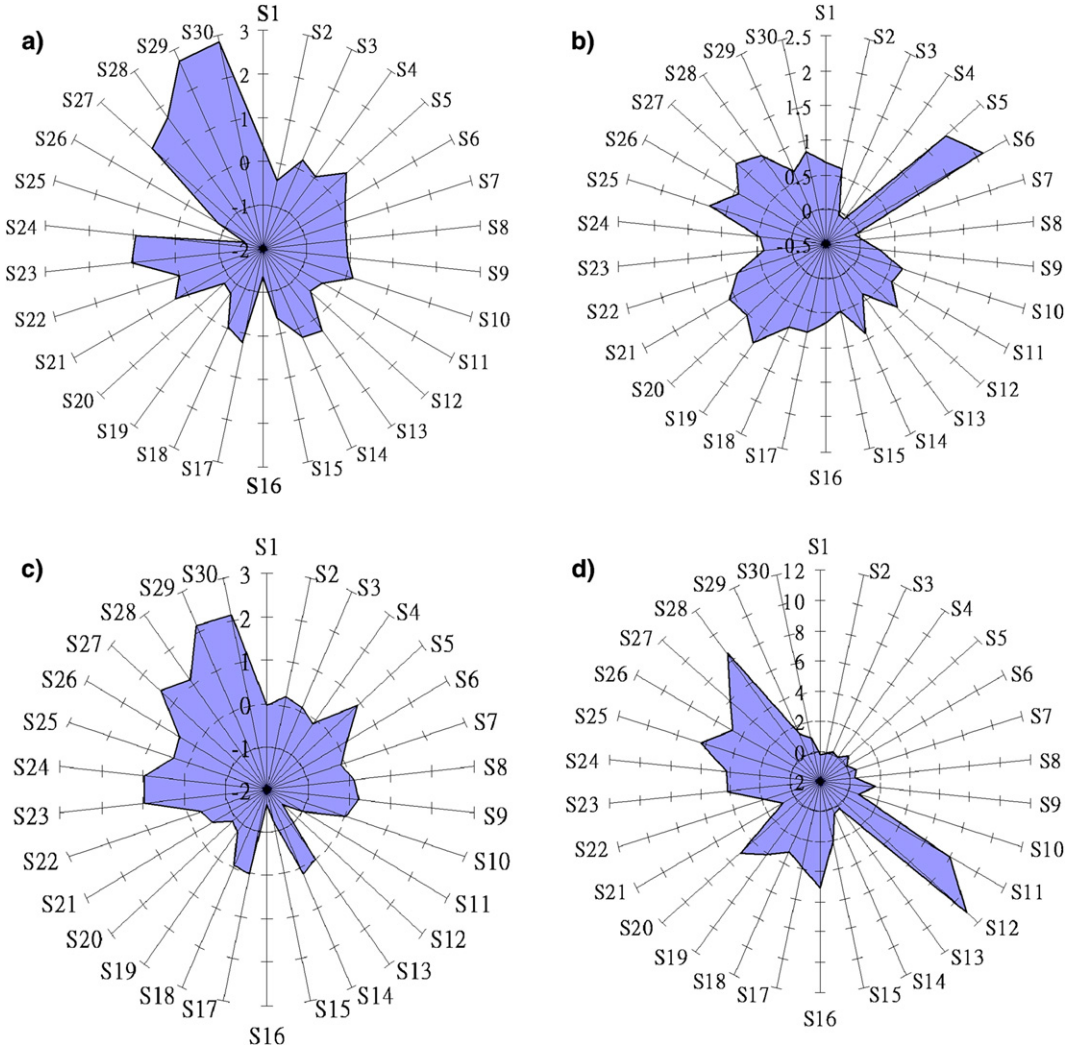

Fig. 5. Radar plots of the room temperature resistance response (△R/R %) of a 30-sensor array for different gases and concentrations in air: (a) DCM (12.3 wt.%), (b) ACN (1.3 wt.%), (c) CEES (1230 ppm), and (d) DMMP (356 ppm) gases.

show resistance changes (△R/R %) for DMMP gas concentrations ranging from 43 ppm to 356 ppm and are shown in Fig. 4. It is obvious that the shapes of the radar plots are similar for different gas concentrations, and the enclosed areas of the plots are proportional to gas concentration. These plots illustrate a significant advantage of this sensor system. An appreciable response can be seen at room temperature, and the intensity of which is comparable with the reported responses observed at higher temperatures for this gas [20].

3.3. Effects of gas type on sensor response and sensing mechanisms

Fig. 5 shows typical radar plots to demonstrate the room temperature resistance response (△R/R %) for an array of 30 sensors (2 sensors for each of 15 sensor types) for different gases and concentrations in air: (a) DCM (12.3 wt.%), (b) ACN (1.3 wt.%), (c) CEES (1230 ppm), (d) DMMP (356 ppm), respectively. It shows that the shapes of the radar plots are significantly different for these four different gases. The reason for such a difference in plot shape may be correlated with interaction activities of gases with resident microstructural differences of these composite gas-sensing materials (CNTs + polymers), e.g., the nature of their attendant chemical functional groups. In general, the sensing behavior of polymers is related to localized molecular interactions with the analyte, including chemical bond formation, surface chemical reactivity, surface dipole interaction, and long-range van der Waals forces. At the molecular level, it was reported that parameters like polymer backbone planarity, side chain length, conjugation length, and structural transformation energy may influence the conductivity [21]. The analyte–polymer interaction most likely modulates one or more of these parameters, thus influencing the surface resistivity intrinsic to the thin film polymer. This implies the possibility that multiple sensing mechanisms may act simultaneously. Upon exposure of a specific polymer to a particular analyte, one mechanism most likely dominates, resulting in the measured resistivity change [22]. These polymers may produce a positive response to polar analytes and a negative response to non-polar analytes. One possible explanation is that the dipole–dipole electrostatic force between polar analytes with certain dipole moments and polymer dipolar alkyl side chains can compress the polymer molecules, thus reducing the hopping distance and associated activation energy.

In other words, Figs. 4 and 5 indicate that the shape and the enclosed area of radar plot depend on gas type and concentration, respectively. The gas specificity of this sensor array was mainly enhanced due to excellent selection of gas sensing materials and device structures. It can be concluded that the radar plots are good fingerprints for these four different toxic gases with concentrations in ppm range.

3.4. Sensor array analyte specificity

From the radar plot data-base for various gases and concentrations, the principal component analysis (PCA) method was used to analyze the gas differentiation and sensing reproducibility. The PCA method essentially reduces a large number of correlated variables to a fewer number of linearly-independent combinations of variables. Fig. 6 shows 3-D PCA plots for four analytes. They clearly demonstrate that the four tested gases are characterized by their own well-defined boundaries, and that the data scatter around three points in each gas boundary is relatively small. In other words, results signify that excellent gas specificity and sensing reproducibility can be achieved for the four tested gases. The first two principal components on the two horizontal axes of Fig. 6 show a high cumulative variance of 94.49%.

4. Conclusions

An array composed of 30 composite bilayer sensors prepared on a Si wafer was fabricated by solution droplet casting MWCNTs followed by one of the 15 functional polymer materials. The experimental results of the radar plots for an array with 30 gas sensor stacks (polymer/MWCNTs/Si wafer) were shown to successfully differentiate among the four tested toxic gases with sensitivity in the ppm concentration range, and their associated PCAs could be used to read the complicated radar plots for different gas types. The resistance variation (△R/R %) for the 43 ppm concentration of the DMMP gas mixture can reach about 1.6% even at room temperature. By monitoring the S/N ratio of the resistance response and carefully controlling the process and environment, the sensitivity much lower than 43 ppm concentration for DMMP gas at room temperature is likely. In conclusion, this MWCNT-assisted chemical gas sensing array can be very helpful for the future development of the integrated gas sensing chip with a “system-on-chip” design.

Acknowledgments

The authors would like to acknowledge the support of the National Science Council of Taiwan under Project Nos. NSC98-2221-E-451-001 and NSC97-2112-M-214-002-MY2. We also would like to thank the CSIST and NCTU for their support on the gas sensing experiments.

References

[1] C. Dekker, Phys. Today 52 (1999) 22.
[2] J. Li, Y. Lu, Q. Ye, M. Cinke, J. Han, M. Meyyappan, Nano Lett. 3 (7) (2003) 929.
[3] T. Someya, J. Small, P. Kim, C. Nuckolls, J.T. Yardley, Nano Lett. 3 (7) (2003) 877.
[4] E. Snow, F. Perkins, E. Houser, S. Badescu, T. Reinecke, Science 307 (5717) (2005) 1942.
[5] W. Gopel, K.D. Schierbaum, Sens. Actuators, B 26 (1–3) (1995) 1.
[6] H. Meixner, J. Gerblinger, U. Lampe, M. Fleischer, Sens. Actuators, B 23 (2–3) (1995) 119.
[7] J.M. Slater, J. Paynter, E. Watt, Analyst 118 (4) (1993) 379.
[8] M.C. Lonergan, E.J. Severin, B.J. Doleman, S.A. Beaber, R.H. Grubb, N.S. Lewis, Chem. Mater. 8 (9) (1996) 2298.
[9] J.W. Gardner, P.N. Bartlett, Sens. Actuators, A 51 (1) (1995) 57.
[10] B.J. Doleman, E.J. Severin, N.S. Lewis, Proc. Natl. Acad. Sci. U. S. A. 95 (10) (1998) 5442.
[11] E.J. Severin, B.J. Doleman, N.S. Lewis, Anal. Chem. 72 (4) (2000) 658.
[12] M.A. Ryan, N.S. Lewis, Enantiomer 6 (2–3) (2001) 159.
[13] C. Hagleitner, A. Hierlemann, D. Lange, A. Kummer, N. Kerness, O. Brand, H. Baltes, Nature 414 (6861) (2001) 293.
[14] M. Penza, M. Alvisi, R. Rossi, E. Serra, R. Paolesse, A. D'Amico, C. Di Natale, Nanotechnology 22 (12) (2011).
[15] L.C. Wang, K.T. Tang, C.T. Kuo, C.L. Ho, S.R. Lin, Y. Sung, C.P. Chang, J. Micro/Nanolithogr. MEMS MOEMS 9 (3) (2010).
[16] Y.S. Kim, S.C. Ha, Y. Yang, Y.J. Kim, S.M. Cho, H. Yang, Y.T. Kim, Sens. Actuators, B 108 (1–2) (2005) 285.
[17] J.W. Grate, S.J. Patrash, M.H. Abraham, Anal. Chem. 67 (13) (1995) 2162.
[18] A. Hierlemann, E.T. Zellers, A.J. Ricco, Anal. Chem. 73 (14) (2001) 3458.
[19] L. Wang, K. Tang, S. Chiu, S. Yang, C. Kuo, Biosens. Bioelectron. 26 (11) (2011) 4301.
[20] A.A. Tomchenko, G.P. Harmer, B.T. Marquis, Sens. Actuators, B 108 (1–2) (2005) 41.
[21] G.R. Hutchison, M.A. Ratner, T.J. Marks, J. Am. Chem. Soc. 127 (7) (2005) 2339.
[22] B. Li, S. Santhanam, L. Schultz, M. Jeffries-El, M.C. Iovu, G. Sauve, J. Cooper, R. Zhang, J.C. Revelli, A.G. Kusne, Sens. Actuators, B 123 (2) (2007) 651.